How orbital angular momentum affects beam shifts in optical reflection

M. Merano, N. Hermosa, and J. P. Woerdman
Huygens Laboratory, Leiden University, P.O. Box 9504, NL-2300 RA Leiden, The Netherlands

A. Aiello
Max Planck Institute for the Science of Light, Günter-Scharowsky-Straße 1/Bau 24, D-91058 Erlangen, Germany

(Received 3 March 2010; published 24 August 2010)

It is well known that reflection of a Gaussian light beam (TEM_{00}) by a planar dielectric interface leads to four beam shifts when compared to the geometrical-optics prediction. These are the spatial Goos-Hänchen (GH) shift, the angular GH shift, the spatial Imbert-Fedorov (IF) shift, and the angular IF shift. We report here, theoretically and experimentally, that endowing the beam with orbital angular momentum leads to coupling of these four shifts; this is described by a 4×4 mixing matrix.

DOI: 10.1103/PhysRevA.82.023817 PACS number(s): 42.79.−e, 41.20.Jb, 42.25.Gy, 78.20.−e

I. INTRODUCTION

The reflection of a light beam by a mirror shows subtle aspects that were first conjectured by Newton [1]: The center of the reflected beam may show a small spatial shift *in* the plane of incidence relative to the position predicted by geometrical optics. This shift has been named after Goos and Hänchen (GH), who were the first to observe it in total internal reflection (TIR) [2]. Additionally, there is a spatial shift *perpendicular* to the plane of incidence, the so-called Imbert-Fedorov shift (IF) [3,4]. There exist also *angular* GH and IF shifts, both of which have been demonstrated recently in external reflection [5,6]. The angular shifts can be seen as shifts in wave-vector space [6–8]. All these shifts depend on the polarization of the incident photons. Accurate calculations of either GH or IF shifts (or both) can be found in Refs. [9–11]. In more recent years the GH shift has been studied in a large diversity of cases, ranging from photonic crystals [12] to neutron optics [13].

We are interested in the question of how these beam shifts are affected when the light beam is endowed with orbital angular momentum (OAM). OAM is a relatively novel degree of freedom of a light beam that can be found in applications from optical tweezers to quantum information science [14,15]. Theoretically, a treatment of the effect of OAM on beam shifts has already been given, first by Fedoseyev [16–18] and then by Bliokh *et al.* [19]. Here we prefer to develop our own theoretical treatment based on straightforward application of Snell's law and the Fresnel equations, in order to derive a unified matrix formalism for the four basic shifts: spatial GH, angular GH, spatial IF, and angular IF. Experimentally, Okuda and Sasada have studied the deformation of an OAM carrying beam using TIR very close to the critical angle [20]; however, they did not report GH and IF shifts. Dasgupta and Gupta have measured the IF shift of an OAM beam reflected by a dielectric interface, but only for the spatial case [21].

It is the purpose of this article to report a theoretical and experimental study of the effect of OAM on the four basic shifts: spatial GH, angular GH, spatial IF, and angular IF. We find that these shifts are coupled by OAM; this is described by an OAM-dependent 4×4 mixing matrix. We have experimentally confirmed this mixed occurrence of GH and IF shifts.

II. THEORY

In this section we furnish a thorough theoretical analysis for the problem of the reflection of an OAM-carrying light beam by a dielectric interface.

Consider a monochromatic beam containing a continuous distribution of wave vectors $\mathbf{k}$ centered around $\mathbf{k}_0 = k_0 \hat{\mathbf{z}}_i$, where $\hat{\mathbf{z}}_i$ is a unit vector along the central propagation direction of the incident beam: $\mathbf{k} = k_0 \hat{\mathbf{k}} = \mathbf{k}_0 + \mathbf{q}$, with $\mathbf{q} = \mathbf{q}_T + q_L \hat{\mathbf{z}}_i$ and $\mathbf{q}_T \cdot \hat{\mathbf{z}}_i = 0$. Using the notation of Fig. 1, we write $q_T/k_0 = \sin\alpha$ and $q_L/k_0 = 1 - \cos\alpha$ with $q_T = |\mathbf{q}_T|$ and $\alpha = \arccos(\hat{\mathbf{k}} \cdot \hat{\mathbf{k}}_0)$. A collimated beam has a narrow distribution of wave vectors around $\mathbf{k}_0$ such that $\sin\alpha \cong \alpha \ll 1$ with $q_T/k_0 \cong \alpha \ll 1$ and $q_L/k_0 \cong (q_T/k_0)^2/2$. Thus, if we write $\mathbf{k} = k_0(\hat{\mathbf{x}}_i U + \hat{\mathbf{y}} V + \hat{\mathbf{z}}_i W)$ with $W = \sqrt{1 - U^2 - V^2}$, we can assume $U, V \ll 1$ without significant error. Let $\mathbf{E}^I(\mathbf{r},t)$ be the electric field of the incident beam. Upon reflection, this field evolves to $\mathbf{E}^R(\mathbf{r},t)$, which is to be found. From the linearity of the wave equation it follows that $\mathbf{E}^R(\mathbf{r},t)$ can be determined by studying the action of the interface upon each plane-wave field,

$$\boldsymbol{A}^I(\mathbf{k}) = \boldsymbol{f}_\perp(\mathbf{k}) \exp(i\mathbf{k} \cdot \mathbf{r} - i\omega t), \tag{1}$$

that constitutes $\mathbf{E}^I(\mathbf{r},t)$, with $\omega = |\mathbf{k}|c$. According to Refs. [22,23], we assume the polarization-dependent amplitude of $\boldsymbol{A}^I(\mathbf{k})$ equal to $\boldsymbol{f}_\perp(\mathbf{k}) = \hat{\boldsymbol{f}} - \hat{\mathbf{k}}(\hat{\mathbf{k}} \cdot \hat{\boldsymbol{f}}) = a_p(\mathbf{k})\, \hat{\boldsymbol{x}}_\mathbf{k} + a_s(\mathbf{k})\, \hat{\mathbf{y}}_\mathbf{k}$, with

$$a_p(\mathbf{k}) = f_p + V f_s \cot\theta, \quad a_s(\mathbf{k}) = f_s - V f_p \cot\theta, \tag{2}$$

up to first order in U, V and $\theta = \arccos(\hat{\mathbf{z}}_i \cdot \hat{\mathbf{z}})$. Here $\hat{\boldsymbol{f}} = f_p \hat{\boldsymbol{x}}_i + f_s \hat{\mathbf{y}}$ is a unit complex vector that fixes the polarization of the incident beam, and $\hat{\mathbf{y}}_\mathbf{v} = \hat{\mathbf{z}} \times \mathbf{v}/|\hat{\mathbf{z}} \times \mathbf{v}|$ and $\hat{\boldsymbol{x}}_\mathbf{v} = \hat{\mathbf{y}}_\mathbf{v} \times \mathbf{v}$ denote a pair of mutually orthogonal real unit vectors that together with the arbitrary vector $\hat{\mathbf{v}} = \mathbf{v}/|\mathbf{v}|$ form a right-handed Cartesian reference frame $K_\mathbf{v} = \{\hat{\boldsymbol{x}}_\mathbf{v}, \hat{\mathbf{y}}_\mathbf{v}, \hat{\mathbf{v}}\}$ attached to $\mathbf{v}$.

When the beam is reflected at the interface, each plane wave evolves as $\boldsymbol{A}^I(\mathbf{k}) \to \boldsymbol{A}^R(\mathbf{k})$, where

$$\boldsymbol{A}^R(\mathbf{k}) = [r_p(\theta_\mathbf{k}) a_p \hat{\boldsymbol{x}}_{\tilde{\mathbf{k}}} + r_s(\theta_\mathbf{k}) a_s \hat{\mathbf{y}}_{\tilde{\mathbf{k}}}] \chi(\tilde{\mathbf{r}}, t) \tag{3}$$

and $\chi(\tilde{\mathbf{r}},t) = \exp(i\tilde{\mathbf{k}} \cdot \mathbf{r} - i\omega t) = \exp(i\mathbf{k} \cdot \tilde{\mathbf{r}} - i\omega t)$. The notation $\tilde{\mathbf{v}}$ indicates the mirror image of the vector $\mathbf{v}$ with

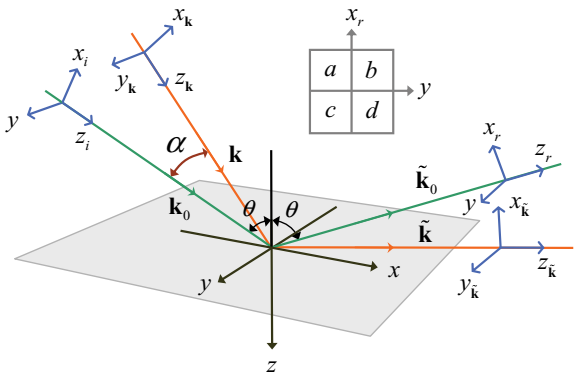

FIG. 1. (Color online) Geometry of beam reflection at a dielectric interface. The reflected wave vector $\tilde{\mathbf{k}}$ is the mirror image of the incident wave vector $\mathbf{k}$. (Inset) Quadrant detector with sensitive areas a, b, c, and d.

respect to the interface: $\tilde{\mathbf{v}} = \mathbf{v} - 2\hat{\mathbf{z}}(\hat{\mathbf{z}}\cdot\mathbf{v})$, with $\tilde{\mathbf{v}}\cdot\mathbf{u} = \mathbf{v}\cdot\tilde{\mathbf{u}}$ [24]. Moreover, $r_p(\theta_\mathbf{k})$ and $r_s(\theta_\mathbf{k})$ are the Fresnel reflection coefficients at incidence angle $\theta_\mathbf{k} = \arccos(\hat{\mathbf{k}}\cdot\hat{\mathbf{z}})$ for p and s waves, respectively. By direct calculation it is not difficult to show that, up to first order in U,V,

$$\hat{\mathbf{x}}_{\tilde{\mathbf{k}}} = \hat{\mathbf{x}}_r - V(\cot\theta)\hat{\mathbf{y}} + U\hat{\mathbf{z}}_r, \tag{4}$$

$$\hat{\mathbf{y}}_{\tilde{\mathbf{k}}} = V(\cot\theta)\hat{\mathbf{x}}_r + \hat{\mathbf{y}} - V\hat{\mathbf{z}}_r, \tag{5}$$

$$r_\lambda(\theta_\mathbf{k}) = r_\lambda + Ur'_\lambda, \tag{6}$$

where $\lambda \in \{p,s\}$, $r_\lambda = r_\lambda(\theta)$, and $r'_\lambda = \partial r_\lambda(\theta)/\partial\theta$. With the use of Eqs. (2) and (4)–(6) in Eq. (3), we obtain

$$\boldsymbol{A}^R(\mathbf{k}) = \hat{\mathbf{x}}_r A_p^R(\mathbf{k}) + \hat{\mathbf{y}} A_s^R(\mathbf{k}) + \hat{\mathbf{z}}_r A_L^R(\mathbf{k}), \tag{7}$$

where, up to first order in U,V,

$$A_\lambda^R(\mathbf{k}) = f_\lambda r_\lambda(1 + iX_\lambda U - iY_\lambda V)\chi(\tilde{\mathbf{r}},t), \tag{8}$$

$$A_L^R(\mathbf{k}) = (f_p r_p U - f_s r_s V)\chi(\tilde{\mathbf{r}},t). \tag{9}$$

Here we have defined

$$X_p = -i\frac{\partial \ln r_p}{\partial\theta}, \quad Y_p = i\frac{f_s}{f_p}\left(1 + \frac{r_s}{r_p}\right)\cot\theta, \tag{10}$$

with $X_s = X_p|_{p\leftrightarrow s}$ and $Y_s = -Y_p|_{p\leftrightarrow s}$. The limit of specular reflection is achieved by letting $r_p \to 1$ and $r_s \to -1$, where Eq. (10) reduces to $X_p = 0 = X_s$ and $Y_p = 0 = Y_s$. Notice that from Eqs. (8) and (9) it follows that for a paraxial beam the longitudinal electric-field energy density $|A_L^R|^2$ scales as $\sim\alpha^2$ and it is therefore negligible with respect to the transverse electric-field energy density $|A_p^R|^2 + |A_s^R|^2$ that scales as $\sim 1 + 2\alpha$. Thus, up to first order in α, we can neglect the longitudinal term $A_L^R(\mathbf{k})$ and write $\boldsymbol{A}^R(\mathbf{k}) \simeq \hat{\mathbf{x}}_r A_p^R + \hat{\mathbf{y}} A_s^R$. Moreover, for small shifts X_λ and Y_λ one can write $1 + iX_\lambda U - iY_\lambda V \simeq \exp(iX_\lambda U - iY_\lambda V)$, and in the Cartesian coordinate system attached to the reflected beam $\chi(\tilde{\mathbf{r}},t) = \exp[i(-UX + VY + WZ)]\exp(-i\omega t)$, with $X = k_0 x_r$, $Y = k_0 y$, and $Z = k_0 z_r$, where z_r is the distance from the waist of the incident beam to the quadrant detector measured along the trajectory of the beam. Thus, Eq. (8) can be rewritten as

$$A_\lambda^R(\mathbf{k}) \simeq f_\lambda r_\lambda \chi(-X + X_\lambda, Y - Y_\lambda, Z, t). \tag{11}$$

The passage from the single plane-wave field $\boldsymbol{A}^R(\mathbf{k})$ to the total electric field $\mathbf{E}^R(\mathbf{r},t)$ is realized by substituting the plane-wave scalar amplitude $\chi(\mathbf{r},t)$ into Eq. (11), with the electric-field scalar amplitude $E(\mathbf{r},t)$ describing the spatial distribution of the incident beam. In the present case, because we want to study the behavior under reflection of OAM beams, we choose $E(\mathbf{r},t) = \psi_\ell(\mathbf{r})\exp(-i\omega t)$, $\psi_\ell(\mathbf{r})$ being the Laguerre-Gauss paraxial field with OAM index $\ell \in \{0, \pm 1, \pm 2, \ldots\}$ and radial index $p = 0$: $\psi_\ell(X,Y,Z) \propto \exp[-(X^2 + Y^2)/(2\Lambda + i2Z)]\,(X + is_\ell Y)^{|\ell|}$, with $s_\ell = \mathrm{sign}(\ell)$ and $\Lambda = k_0(k_0 w_0^2/2)$ denoting the dimensionless Rayleigh range of the beam with waist w_0 [25]. Thus, the transverse electric field of a Laguerre-Gauss beam reflected by a plane interface can be written as

$$E_\lambda^R(\mathbf{r},t) \simeq f_\lambda r_\lambda \psi_\ell(-X + X_\lambda, Y - Y_\lambda, Z)\exp(-i\omega t). \tag{12}$$

In this expression the terms X_λ and Y_λ are responsible for the GH [8] and IF [19] shifts of the center of the beam, respectively. These displacements can be assessed by measuring the position of the center of the reflected beam with a quadrant detector centered at $x_r = 0, y = 0$ along the reference axis z_r attached to the reflected central wave vector $\tilde{\mathbf{k}}_0 = k_0\hat{\mathbf{z}}_r$. A quadrant detector has four sensitive areas, denoted a, b, c, and d in the inset of Fig. 1, each delivering a photocurrent I_a, I_b, I_c, and I_d, respectively, when illuminated. The two currents $I_x = (I_a + I_b) - (I_c + I_d)$ and $I_y = (I_b + I_d) - (I_a + I_c)$ are thus proportional to the x and the y displacement of the beam intensity distribution relative to the center of the detector, respectively.

If $\ell = 0$, $\psi_0(-X + X_\lambda, Y - Y_\lambda)$ reduces to a shifted fundamental Gaussian beam, and in the hypothesis of small deviations $X_\lambda, Y_\lambda \ll 1$, a straightforward calculation furnishes

$$\frac{I_x}{I} = N_0\left(\Delta_{\mathrm{GH}} + \frac{Z}{\Lambda}\Theta_{\mathrm{GH}}\right), \quad \frac{I_y}{I} = N_0\left(\Delta_{\mathrm{IF}} + \frac{Z}{\Lambda}\Theta_{\mathrm{IF}}\right), \tag{13}$$

where $I = I_a + I_b + I_c + I_d$ and $N_0 = \sqrt{2/(\pi\sigma^2)}$, with $\sigma^2 = (\Lambda/2)\sqrt{1 + Z^2/\Lambda^2}$. Here we have defined the two spatial (Δ) and the two angular (Θ) shifts,

$$\Delta_{\mathrm{GH}} = \sum_{\lambda=p,s} w_\lambda \mathrm{Re}(X_\lambda), \quad \Delta_{\mathrm{IF}} = \sum_{\lambda=p,s} w_\lambda \mathrm{Re}(Y_\lambda), \tag{14}$$

and

$$\Theta_{\mathrm{GH}} = \sum_{\lambda=p,s} w_\lambda \mathrm{Im}(X_\lambda), \quad \Theta_{\mathrm{IF}} = \sum_{\lambda=p,s} w_\lambda \mathrm{Im}(Y_\lambda), \tag{15}$$

respectively, where the non-negative coefficients w_λ are defined as the fraction of the electric-field energy with polarization $\lambda = p,s$ in the reflected beam:

$$w_\lambda \equiv \frac{|r_\lambda f_\lambda|^2}{|r_p f_p|^2 + |r_s f_s|^2}. \tag{16}$$

If $\ell \neq 0$, Eq. (13) becomes

$$\frac{I_x}{I} = N_\ell\left(\Delta_{\mathrm{GH}}^\ell + \frac{Z}{\Lambda}\Theta_{\mathrm{GH}}^\ell\right), \quad \frac{I_y}{I} = N_\ell\left(\Delta_{\mathrm{IF}}^\ell + \frac{Z}{\Lambda}\Theta_{\mathrm{IF}}^\ell\right), \tag{17}$$

where $N_\ell = N_0\Gamma(|l|+1/2)/\left[\Gamma(|l|+1)\sqrt{\pi}\right]$ [$\Gamma(x)$ denotes the Γ function] and

$$\begin{bmatrix} \Delta^\ell_{\mathrm{GH}} \\ \Theta^\ell_{\mathrm{IF}} \\ \Delta^\ell_{\mathrm{IF}} \\ \Theta^\ell_{\mathrm{GH}} \end{bmatrix} = \begin{bmatrix} 1 & -2\ell & 0 & 0 \\ 0 & 1+|2\ell| & 0 & 0 \\ 0 & 0 & 1 & 2\ell \\ 0 & 0 & 0 & 1+|2\ell| \end{bmatrix} \begin{bmatrix} \Delta_{\mathrm{GH}} \\ \Theta_{\mathrm{IF}} \\ \Delta_{\mathrm{IF}} \\ \Theta_{\mathrm{GH}} \end{bmatrix}. \quad (18)$$

Equation (18) clearly displays the mixing between spatial and angular GH and IF shift, occurring only for $\ell \neq 0$, and it is in agreement with the results presented in Ref. [19], apart from the factor "2" in front of ℓ [26]. Notice that the polarization dependence of the four ℓ-dependent shifts on the left side of Eq. (18) resides in the four ℓ-independent shifts on the right side of the same equation. It turns out that the 4×4 mixing matrix itself is polarization independent. It should be noticed that in TIR, in contrast to partial reflection, both GH and IF angular shifts Θ_{GH} and Θ_{IF} are identically zero since the Fresnel coefficients are purely imaginary [27]. Thus, in this case it follows from Eq. (18) that mixing vanishes.

III. EXPERIMENTAL SETUP

Our experimental setup is shown in Fig. 2. A home-built HeNe laser ($\lambda_0 = 633$ nm) is forced to operate in a single higher-order Hermite-Gaussian (HG_{nm}) mode with $m = 0$ by insertion of a 40-μm-diameter wire normal to the axis of the laser cavity [28]. The HG_{n0} beam is sent through an astigmatic mode converter consisting of two cylinder lenses, with their common axis oriented at 45° relative to the intracavity wire. This introduces a Gouy phase which converts the HG_{n0} beam to a $\mathrm{LG}_{\ell p}$ beam with $\ell = n$ and $p = 0$ [28]. Lenses 1 and 2 are used for mode matching; the beam leaving lens 2 is collimated with a waist parameter $w_0 = 775$ μm, a power of typically 600 μW, and a polarization set by a linear polarizer. We have incorporated the option to greatly enhance the angular spread of the beam by inserting lens 3 ($f = 70$ mm), leading to $w_0 = 19$ μm. Either with or without lens 3 present, the beam is externally reflected by the base plane of a glass prism (BK7, $n = 1.51$). We measured the polarization-differential shifts of the reflected $\mathrm{LG}_{\ell 0}$ beam with a calibrated quadrant detector. We also obtained these shifts for the fundamental LG_{00} beam

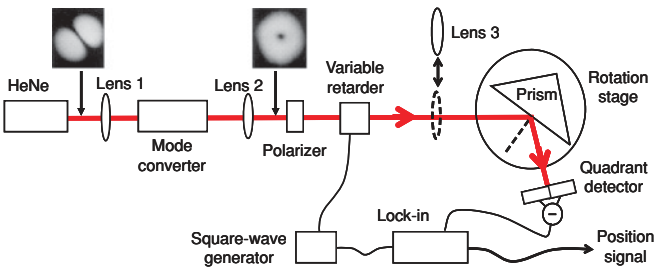

FIG. 2. (Color online) Experimental setup. The insets show the HG_{10} and LG_{10} mode profiles. The quadrant detector measures the OAM-controlled shift of the reflected beam in the plane of incidence (GH shift) and perpendicular to it (IF shift). Both the GH shift and the IF shift have a spatial and an angular contribution. See text for further details.

(=TEM_{00}) by simply removing the intracavity wire from the HeNe laser.

It follows from Eqs. (13)–(17) that using a collimated incident beam, that is, $\Lambda \gg Z$, leads to total predominance of the spatial shift. On the other hand, the use of a focused beam, that is, $\Lambda \ll Z$, leads to total predominance of the angular shift. These two extreme cases were realized in our experiment by the removal (respectively, insertion) of lens 3. Specifically, the value of the Rayleigh range $L = k_0 w_0^2/2$ was 2.96 m and 1.8 mm, respectively; as standard we have chosen the distance z_r between the beam waist and the quadrant detector to be 9.5 cm. We experimentally checked the angular nature of the shift (where expected) by verifying that the detector signal depended linearly on changes in z_r.

We performed all measurements by periodically (2.5 Hz) switching the polarization of the incident beam with a liquid-crystal variable retarder and synchronously measuring (with a lock-in amplifier) the relative beam position for one polarization with respect to the other [5,29]. Experimentally, we were restricted to using the first-order LG modes ($\ell = \pm 1$) by the low gain of the HeNe laser.

IV. EXPERIMENTAL RESULTS AND COMPARISON WITH THEORY

Our experimental results for the polarization-differential shifts versus the angle of incidence are reported in Fig. 3, together with the theoretical curves ($\ell = 0$ and $\ell = \pm 1$) which are based upon Eqs. (13)–(17). The four panels show the spatial and angular varieties of GH and IF shifts. Note that we have plotted here the true GH and IF shifts Δ/k_0 and

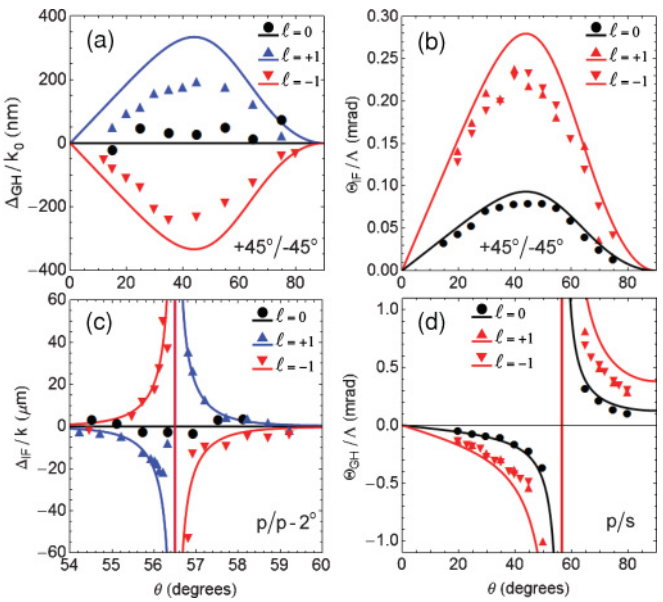

FIG. 3. (Color online) Reflective beam shift for partial dielectric reflection from an air-glass interface as a function of the angle of incidence. Plotted curves are the theoretical polarization-differential shifts for the two polarizations indicated in each panel. Experimental data and theoretical curves refer to $\ell = 0$ and $\ell = \pm 1$. The panels display the spatial GH shift (a), angular IF shift (b), spatial IF shift (c), and angular GH shift (d). Here $k_0 = 2\pi/\lambda_0$; see text for further details.

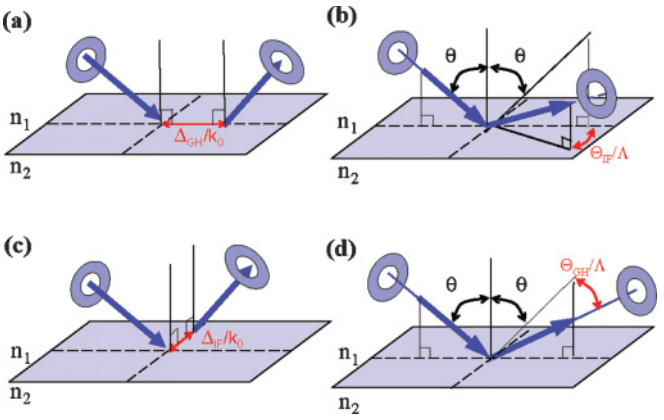

FIG. 4. (Color online) Reflection of an OAM-carrying Laguerre-Gaussian (LG) beam at a dielectric interface. Depending on the input polarization, this may lead to a longitudinal shift (GH effect) or to a transverse shift (IF effect), where longitudinal and transverse refer to the plane of incidence. Each of these shifts consists of a spatial part and an angular part, which are observed, respectively, in the near field and in the far field of the LG beam. The magnitude of the shifts increases with the OAM index ℓ. (a) The spatial GH effect; (b) the angular IF effect; (c) the spatial IF effect; (d) the angular GH effect. Note that Δ and Θ are dimensionless quantities; Λ and k_0 are the dimensionless Rayleigh range and the wave number of the LG beam, respectively. See text for further details.

Θ/Λ, respectively, and not the dimensionless shifts Δ and Θ. In each individual case the polarization modulation basis has been chosen so as to maximize the magnitude of the OAM effect.

Figure 4 shows a cartoonlike representation of the four cases that we address.

The overall agreement between experiment and theory is reasonable if we realize that there is no fitting parameter involved; we ascribe the remaining discrepancies to insufficient modal purity of the LG_{10} beam (we are very sensitive to this since we use a quadrant detector).

Figure 3(a) shows the spatial GH shift for a polarization basis of diagonal linear polarizations. In this case, the GH shift is absent for $\ell = 0$ but it appears for $\ell = \pm 1$; the sign of the shift reverses when going from $\ell = +1$ to $\ell = -1$. In Fig. 3(b) we show that the angular IF shift is different for $\ell = 0$ and $\ell = \pm 1$, using again diagonal linear polarizations. No difference occurs for $\ell = +1$ versus $\ell = -1$. Proceeding to Fig. 3(d) we observe an angular GH shift when using a linear polarization basis (s, p) for both $\ell = 0$ and $\ell = \pm 1$. Both cases show a dispersive resonance at the Brewster angle; for $\ell = 0$ these experimental results have been reported recently [5], whereas the data for $\ell = \pm 1$ (with opposite sign for $\ell = +1$ and $\ell = -1$) are new. Figure 3(c) shows the OAM dependence of the spatial IF shift, observed in a linear polarization basis $(p, p - 2^\circ)$ [21,30]. Here the shift is zero for $\ell = 0$, whereas it shows a dispersive Brewster resonance for $\ell = \pm 1$ (with opposite sign for $\ell = +1$ and $\ell = -1$).

Finally, we have confirmed experimentally that OAM did not affect spatial and angular GH and IF shifts in the TIR case (not shown); TIR was realized by flipping the glass prism in Fig. 2.

V. CONCLUSIONS

We have presented a unified theoretical description of how the OAM of a light beam affects its kinematic degrees of freedom when the beam is reflected by a dielectric interface. Without OAM the reflection leads to four beam shifts relative to geometrical optics, namely, the GH and IF shifts, each of which may have a positional and an angular part. We introduce a 4×4 polarization-independent (but ℓ-dependent) coupling matrix that describes the OAM-induced mixing of these four shifts when using a quadrant detector. Experimentally, we have confirmed this theory by measuring the four shifts as a function of the angle of incidence, for OAM values $\ell = 0$ and ± 1. We have observed for the first time the OAM-induced spatial GH shift as well as the OAM-affected angular GH and IF shifts [see Figs. 3(a)–3(c)]. Extension of all this from reflection to transmission (i.e., refraction) is straightforward.

Understanding these effects is important since they generally affect control of OAM beams by mirrors and lenses. The angular shifts are particularly interesting from a metrology point of view, both classically and quantum mechanically, since the corresponding transverse excursion of the beam center grows without limits when the beam propagates; this greatly promotes its detectability [5,31].

ACKNOWLEDGMENTS

We thank K. Y. Bliokh for stimulating us to measure the OAM-induced GH shift which acted as the seed of this article. Our work is part of the program of the Foundation for Fundamental Research of Matter (FOM). It is also supported by the European Union within FET Open-FP7 ICT as part of the STREP Program 255914 PHORBITECH. A.A. acknowledges support from the Alexander von Humboldt Foundation.

[1] I. Newton, *Opticks* (reprinted by Dover, New York, 1952); see Query 4 on p. 339.
[2] F. Goos and H. Hänchen, Ann. Phys. (Leipzig) **436**, 333 (1947).
[3] C. Imbert, Phys. Rev. D **5**, 787 (1972).
[4] F. I. Fedorov, Dokl. Akad. Nauk SSSR **105**, 465 (1955).
[5] M. Merano, A. Aiello, M. P. van Exter, and J. P. Woerdman, Nat. Photonics **3**, 337 (2009).
[6] O. Hosten and P. Kwiat, Science **319**, 787 (2008).
[7] K. Y. Bliokh, A. Niv, V. Kleiner, and E. Hasman, Nat. Photonics **2**, 748 (2008).
[8] A. Aiello and J. P. Woerdman, Opt. Lett. **33**, 1437 (2008).
[9] K. Artmann, Ann. Phys. (Leipzig) **2**, 87 (1948).
[10] K. Y. Bliokh and Y. P. Bliokh, Phys. Rev. Lett. **96**, 073903 (2006).
[11] K. Y. Bliokh and Y. P. Bliokh, Phys. Rev. E **75**, 066609 (2007).

[12] D. Felbacq, A. Moreau, and R. Smaali, Opt. Lett. **28**, 1633 (2003).
[13] V-O. de Haan, J. Plomp, T. M. Rekveldt, W. H. Kraan, A. A. van Well, R. M. Dalgliesh, and S. Langridge, Phys. Rev. Lett. **104**, 010401 (2010).
[14] A. Mair, A. Vaziri, G. Weihs, and A. Zeilinger, Nature (London) **412**, 313 (2001).
[15] H. He, M. E. J. Friese, N. R. Heckenberg, and H. Rubinsztein-Dunlop, Phys. Rev. Lett. **75**, 826 (1995).
[16] V. G. Fedoseyev, Opt. Commun. **193**, 9 (2001).
[17] V. G. Fedoseyev, J. Phys. A **41**, 505202 (2008).
[18] V. Fedoseyev, Opt. Commun. **282**, 1247 (2009).
[19] K. Y. Bliokh, I. V. Shadrivov, and Y. S. Kivshar, Opt. Lett. **34**, 389 (2009).
[20] H. Okuda and H. Sasada, J. Opt. Soc. A **25**, 881 (2008).
[21] R. Dasgupta and P. K. Gupta, Opt. Commun. **257**, 91 (2006).
[22] Y. Fainman and J. Shamir, Appl. Opt. **23**, 3188 (1984).
[23] A. Aiello, C. Marquardt, and G. Leuchs, Opt. Lett. **34**, 3160 (2009).
[24] R. F. Gragg, Am. J. Phys. **56**, 1092 (1988).
[25] L. Mandel and E. Wolf, *Optical Coherence and Quantum Optics*, 1st ed. (Cambridge University Press, Cambridge, UK, 1995).
[26] Here we quantify the GH and IF shifts via the photocurrents I_x/I and I_y/I delivered by the quadrant detector actually used in the experiment, respectively. This furnishes the *median* of the beam intensity distribution. Conversely, in Ref. [19] the same displacements are quantified via the *mean* of the intensity distribution. The difference between these two methods leads to both the trivial prefactor N_ℓ (experimentally eliminated by a detector calibration procedure) and the terms "2ℓ" (instead of "ℓ") in the mixing matrix (18).
[27] A. Aiello, M. Merano, and J. P. Woerdman, Phys. Rev. A **80**, 061801(R) (2009).
[28] M. W. Beijersbergen, L. Allen, H. E. L. O. van der Veen, and J. P. Woerdman, Opt. Commun. **96**, 123 (1993).
[29] M. Merano, A. Aiello, G. W. 't Hooft, M. P. van Exter, E. R. Eliel, and J. P. Woerdman, Opt. Express **15**, 15928 (2007).
[30] In this case maximum modulation of the beam shift is achieved by switching the (linear) polarization beween p and s. However, instead of this we have chosen to switch the polarization between p and $p - 2^\circ$. This was done to reduce the very large intensity contrast occurring during $p \leftrightarrow s$ modulation and thus to minimize a parasitic cross-effect on the displacement as synchronously measured by the quadrant detector.
[31] N. Treps, N. Grosse, W. P. Bowen, C. Fabre, H.-A. Bachor, and P. K. Lam, Science **301**, 940 (2003).